Article

One-Dimensional "Ghost Imaging" in Electron Microscopy of Inelastically Scattered Electrons

Enzo Rotunno,[∇] Simone Gargiulo,[∇] Giovanni M. Vanacore, Chen Mechel, Amir H. Tavabi, Rafal E. Dunin-Borkowski, Fabrizio Carbone, Ivan Madan, Stefano Frabboni, Tugrul Guner, Ebrahim Karimi, Ido Kaminer, and Vincenzo Grillo*

Read Online

ACCESS | Metrics & More | Article Recommendations | Supporting Information

ABSTRACT: Entanglement and correlation are at the basis of quantum mechanics and have been used in optics to create a framework for "ghost imaging". We propose that a similar scheme can be used in an electron microscope to exploit the correlation of electrons with the coincident detection of collective mode excitations in a sample. In this way, an image of the sample can be formed on an electron camera even if electrons never illuminated the region of interest directly. This concept, which can be regarded as the inverse of photon-induced near-field electron microscopy, can be used to probe delicate molecules with a resolution that is beyond the wavelength of the collective mode.
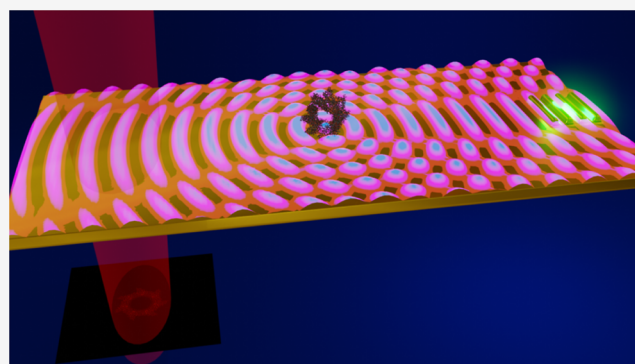
INTRODUCTION

In quantum mechanics, entanglement and correlation are ubiquitous phenomena that are the basis of interacting quantum systems. They have a deep connection to a heavily debated and elusive phenomenon, which is commonly referred to as the "collapse of the wavefunction." This concept describes a loss of quantum information of a non-unitary transformation of a wavefunction while it interacts with a measuring system. For instance, when a quantum particle (QP) interacts with a macroscopic measuring device (MD), they become fully correlated in their interacting degrees of freedom, while other quantum features of the system (i.e., the QP and MD) are unaffected. Therefore, summing ("tracing over") the MD's degrees of freedom results in a loss of information about the device and particle quantum state.[1−4]

In electron microscopy, the inelastic interaction of electrons with matter provides an ideal model system for testing the phenomenology of loss of coherence.[5−13] Inelastic scattering can be observed using electron energy-loss measurements and offers a variety of possibilities in terms of position localization of a wavefunction.[14] Of particular interest here are interactions in the low energy-loss regime, in which excitations include collective modes such as plasmons, polaritons, magnons, and phonons, which have relatively long lifetimes for propagation in a sample. A (joint) measurement performed on the collective modes and electrons provides a unique way to infer the state of the sample. In fact, instead of simply

monitoring the loss of coherence of an electron wavefunction following inelastic scattering, by considering the sample and the electron probe as a correlated system,[15] one can extract more information about the sample and the probe by performing a joint measurement. We obtain the counterintuitive result that, under appropriate conditions, an image of part of the sample is formed on an electron detector even though the electron never interacted with that part of the sample, which was instead explored by travelling collective modes that are correlated with the electron.

"Ghost imaging" is based on the concept of joint measurement,[16] which originally emerged from the studies of the Einstein−Podolsky−Rosen (EPR) paradox.[17−20] Subsequently, it was proved that classically correlated states obtained using raster scanning and joint measurements can also provide ghost imaging.[21] As the superposition principle allows a quantum system to be in different eigenstates simultaneously, many outcomes of the evolution of a given quantum state are possible. However, when the outcome of a classical measurement is defined, one specific evolution is singled out and
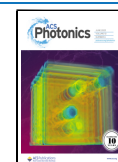
becomes the "real" one as a result of decoherence or state post-selection. When two QPs (in our case an electron and a collective mode) are entangled, their quantum state is not factorized. Therefore, a measurement performed on one particle can reveal the other particle's state, giving rise to seemingly paradoxical effects.[22,23]

In optical "ghost imaging,"[24,25] an entangled photon pair (or classically correlated photons) is sent along two paths. One follows a path where the object and a bucket detector are located consecutively, while the other is sent to a spatially resolved detector such as a charge-coupled device (CCD) camera. The CCD camera is activated only when the bucket detector is hit by the twin photon in coincidence, resulting in the formation of an image on the CCD camera based on this joint measurement. The counter-intuitive result is that an image of the sample is formed on the CCD camera even if such a photon never passed through the sample. This phenomenon can be explained by considering the time inversion of rays emanating from the bucket, going through the sample/object, and reaching the bifurcation where the information reaches the second photon.[24]

RESULTS

Electron Photon Joint Measurements. In order to carry out a similar experiment with electrons, one can utilize the excitation of surface plasmon polaritons (SPPs) in electron scattering and consider how a joint measurement between the SPP and electron states can give rise to an image formed by the electron beam from the evolution of SPPs. Similarly, to the optical counterpart, the electron is detected using a spatially resolved camera. The SPPs traverse through an object, they are converted to photons by means of a localized grating, and they are finally detected by a bucket detector. The signal from the bucket detector (SPPs) triggers the camera, resulting in the formation of a ghost image on the electron beam side.

Coherent dynamics of collective modes in electron microscopy have previously been studied using ultrafast transmission electron microscopy (UTEM).[26,27] This technique involves femtosecond laser excitation synchronized with a pulsed electron probe. The laser-driven electron sources that are needed for such experiments are limited in their coherence and brightness. When adopting a UTEM variant called PINEM (photon-induced near-field electron microscopy), an optically induced near-field excitation can be probed by a simultaneous electron pulse. By systematically changing the delay time between the repeated electron pulse and the stroboscopic excitation, it is then possible to obtain dynamical study[26−28] of such a collective-excitation and induce electron beam shaping mediated by light.[29]

The concept of SPP-electron joint measurement is complementary to PINEM, and it is explored here by considering a thin slab of metal that can support the propagation of SPPs. The electron beam propagates along the z direction, which is perpendicular to the slab. The SPPs lie in the x−y plane. In the x direction, a discontinuous obstacle that takes the form of a double slit is inserted.[30] A more general version of this thought experiment involves replacing the slits by objects that affect the SPP amplitude and phase.

Our approach relies on a joint measurement scheme based on correlation between collective modes and an electron. The coincidence can be achieved using coherent cathodoluminescence (CL) and can be regarded as the time reversal of a pump−probe process.

In this experiment, an SPP is generated by electrons in the left part of the slab (Figure 1a) and converted into light
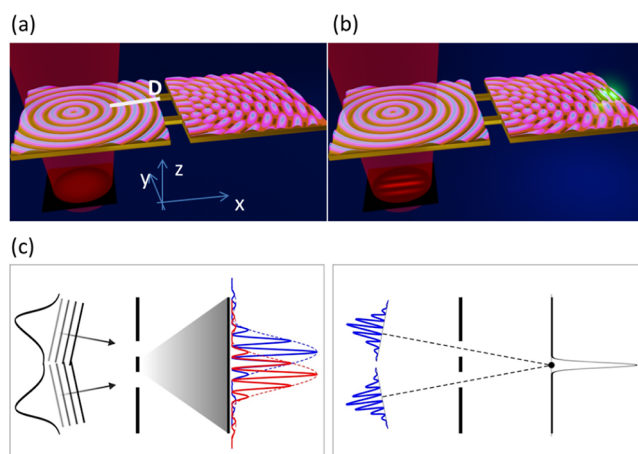

Figure 1. Joint measurement concept. (a) Electron beam impinges on a metallic slab and produces a SPP propagation along its surface. The SPP is scattered by a double slit feature and produces an incoherent sum of many interference patterns, one for each SPP momentum. The image formed on the camera is a truncated Gaussian. (b) Conversion of the SPP to a photon using a suitable optical grating defines the joint wavefunction between the specific SPP mode and the electron state imaged on the electron detector. The image formed by the joint measurement on the electron beam side is a diffraction pattern from the double slit. (c) Left panel shows the propagation and interference of two forward wave components with two particular wavevectors extracted from all of the wavelet components associated with the generated SPP. The right panel shows the reverse wave components of the SPP associated with the point source, representing the corresponding coincident photon scattered from the grating.

through a grating positioned in the right part of the slab (Figure 1b). The grating permits the SPP to be out-coupled by breaking translational symmetry and adding momentum proportional to the grating spatial frequency—such that each quantum of the SPP is transformed into a free-space-propagating photon.[31] The grating provides spatial localization and energy selectivity of the joint measurement. The grating is confined in a region of lateral size Δy, which allows the sample to be resolved in the y direction. Each spatially resolved point in the y direction contains integrated information along the x direction, such as thickness (i.e., extension along the x axis). If a technique such as CL is used to detect the emitted photon, then the grating can be considered as a bucket detector and the two slits as the sample. Care is needed to detect only a specific energy and direction of the photon from the grating.

We infer the image of the two slits or the image of the Fraunhofer interference pattern, which should be formed on the CCD camera for different defocus values, corresponding to conjugate planes of electron propagation after the interaction.

Mathematical Description. In order to demonstrate the feasibility of the approach and to assess its limits, we begin with a description of the SPP in quantum mechanical terms. As basis of correlation, we assume that the overall in-plane momentum of the electrons and SPP is conserved. The joint wavefunction of the SPP and the scattered electron can then be written in the following form:

$$|\Psi\rangle = \sum_{\bar{k},\mathrm{w}} a_{\bar{k}} E^{\mathrm{FWD}}(\bar{k}, \omega) \otimes |\psi_e(-\bar{k}, \varepsilon - \hbar\omega)\rangle \tag{1}$$

where $E^{\text{FWD}}(\overline{k})$ is a specific component of the SPP electric field and ψ_e is the electron wavefunction. In eq 1, $\overline{k}$ is the SPP momentum and the scattered electron recoils by $-\overline{k}$. The decomposition factor $a_{\overline{k}}$ depends on the illumination conditions and the coupling. Energy conservation is written explicitly, such that the energy of the created SPP (given by $\hbar\omega$) corresponds to the energy loss experienced by the swift electron (initially at ε). The superscript FWD stands for "forward" and indicates that the SPP wave propagates in the metal starting from the electron injection region.

The system wavefunction $|\Psi\rangle$ represents a pure state as long as the impinging electron is a pure state. In the following examples, the electron beam is assumed to be monochromatic on a scale of 100 meV, which is within current experimental capabilities. (In general, the uncertainty in electron energy must only be smaller than the energy of the collective mode). The extent to which $|\Psi\rangle$ remains a pure state after scattering is currently at the center of debate in the time-resolved community. Recent contributions show that this can be the case.[32−37] It is assumed below that such a condition can be created. Moreover, the treatment can be generalized to partially coherent beams, while it would fail in the case of a strongly incoherent effect in the propagation of the collective mode.

In eq 1, the SPP wave is treated using classical fields, instead of a more complete second quantization approach.[32] This does not limit the generality of the conclusions, since the SPP probability distribution is unaltered in the proposed experiment. More explicitly, the excitation of a single SPP is considered, which is normally the case and can be achieved by appropriately tuning the coupling strength.[38] To a first approximation, it is sufficient to consider a comparison with the PINEM process.

In PINEM, SPPs generated by the swift electron are neglected, as their population is much lower than those generated by the laser.[39] It is, therefore, reasonable to assume that the main problem of the present joint measurement technique, when compared to direct PINEM, is the small number of events. However, in comparison to PINEM, the greater brightness of a continuous cathode than a pulsed photocathode, which generates significantly fewer electrons, provides partial compensation. We also consider the generated SPP for a well-defined energy, which can be ensured by appropriate detection of the photon energy.

Another consequence of using a semiclassical description of the field is that quantization of the collective excitation is hidden. This creates a problem, since a joint measurement between the photon and electron is possible only in a quantized field framework. We, therefore, rewrite the problem in terms of projection between final and initial states to highlight the contribution of each partial wave to the SPP, so that the coincident measurement arises naturally.

We start from a textbook treatment of the excitation of plasmons by swift electrons. Each electron produces an electric field[40] that can be described by the following expression:

$$\overline{E}_S = \frac{2e\omega}{v^2\gamma\varepsilon}\left[\frac{i}{\gamma}K_0\left(\frac{\omega\rho}{v\gamma}\right)\hat{z} - K_1\left(\frac{\omega\rho}{v\gamma}\right)\hat{\rho}\right] \tag{2}$$

where $K_{0,1}$ are modified Bessel functions of the second kind of order 0 and 1, v is the electron velocity, γ is the relativistic factor for electrons of energy ε, ω is the selected photon frequency, and $\hat{\rho}$ and $\hat{z}$ are unit vectors along the ρ and z

directions in cylindrical coordinates (ρ, ϕ, z). Although the spectrum of temporal frequencies is broadly distributed, we select a single frequency corresponding to the excitation of a specific SPP. The form of the electric field (and the related magnetic field) reflects the distribution of the generated SPP, such that the highly peaked (diverging) function described by eq 2 can be considered as a virtual plasmon source.

From eq 2, we retrieve the characteristic size of the source distribution $s_0 = v\gamma/\omega$. However, we will consider a relatively large electron beam waist with size $s \gg s_0$ as the effective SPP source. For a fixed $\overline{k}$, the ansatz for the initial wave is taken as follows:

$$E(\overline{\rho}) = S_{kS}(\overline{\rho})e^{i\overline{k}\cdot\overline{\rho}} \tag{3}$$

We also assume that $S_{kS}(\overline{\rho})$ has a Gaussian-like distribution with a different center for the allowed values of $\overline{k}$.[15] According to eq 3, the source is a series of truncated "1D plane waves" (confined in the slab) originating from the injection area. The SPP is locked in a transverse magnetic (TM) mode and is treated here as a scalar wave, neglecting polarization-dependent effects. Figure 1c (left) shows a forward-propagating SPP field $E^{\text{FWD}}(\overline{k}, \overline{\rho})$ for a given frequency, propagating from the electron injection region. Each value of $\overline{k}$ results in a different diffraction figure on the right. For the SPP, the double slit has the transfer function $T(y) = \text{Rect}_b(y - d/2) + \text{Rect}_b(y + d/2)$, where d is the distance between the slits, b is the size of the slits, and Rect_b is a support function of size b. The intensity of the joint measurement can be evaluated as projection of the forward-propagating SSP $E^{\text{FWD}}(\overline{k}, \overline{\rho})$ onto states that correspond to a certain detection outcome. The detection probability is defined by a projection of the field (in this case the SPP) on a well-defined position corresponding to the grating. Since the problem is solved in the frequency domain, it becomes similar to a time-independent Schrödinger equation, with the solutions defined in the full domain. States with well-defined arrival points P are eigenstates of the SPP wave equation in the metal slab, since they would exist as solutions of the time-reversal Maxwell equations with a source located at P (Figure 1c, right), thereby providing a way to numerically calculate the fields $E^{\text{REV}}(\overline{k}, \overline{\rho}_{\text{SPP}})$ by solving the reverse problem.

The probability of a certain outcome is determined by the superposition integral between the forward propagating wave $E^{\text{FWD}}(\overline{k}, \overline{\rho}_{\text{SPP}})$ and the time-reversal field $E^{\text{REV}}(\overline{k}', \overline{\rho}_{\text{SPP}})$, according to the expression

$$c = \int E^{\text{FWD}}(\overline{k}, \overline{\rho}_{\text{SPP}})E^{\text{REV}}(\overline{k}', \overline{\rho}_{\text{SPP}})d\overline{\rho}_{\text{SPP}} \tag{4}$$

The partial projection of the total wave function Ψ for the electron-SPP system (eq 1) on the specific SPP outcome is, therefore,

$$|\psi_e(\overline{\rho}_e)\rangle = \left[\int \Psi \cdot E^{\text{REV}}(\overline{k}; \overline{\rho}_{\text{SPP}})d\overline{\rho}_{\text{SPP}}\right] \tag{5}$$

The qualitative shape of the $E^{\text{REV}}(\overline{k}; \overline{\rho}_{\text{SPP}})$ wave is described in Figure 1c (right). From a quantitative perspective, $E^{\text{REV}}(\overline{k}; \overline{\rho}_{\text{SPP}})$ is defined piecewise in the two domains (left and right sides of the double slit feature). At the slit position, the form of E^{REV} is described by a configuration where the spherical wave, reverse-propagating from the bucket detector,

reduces to two plane waves with wave vectors $\overline{k_{1,2}} = |K|(\widehat{\Delta\rho_{1,2}})$, where $\widehat{\Delta\rho_{1,2}}$ is a unitary vector from the jointly measured point to each slit. At the slit position

$$E^{\text{REV}} \approx \delta(\overline{k} - \overline{k_1})\text{Rect}_b\left(y - \frac{d}{2}\right)$$
$$+ \exp(i\varphi)\delta(\overline{k} - \overline{k_2})\text{Rect}_b\left(y + \frac{d}{2}\right) \quad (6)$$

where the phase φ depends on the post-selection position with respect to the slits. In the slits, superposition between E^{REV} and E^{FWD} is possible only if $\overline{k}$ is assumed to be one of the specific values $\overline{k_{1,2}}$. After the SPP state is measured using the bucket detector, the electron becomes a coherent superposition of two pure state

$$|\psi_e(\overline{\rho_e})\rangle = a_1 c_1 |\psi_e(-\overline{k_1}; \overline{\rho_e})\rangle + a_2 c_2 \exp(i\varphi)|\psi_e(-\overline{k_2}; \overline{\rho_e})\rangle \quad (7)$$

where $|\psi_e\rangle$ can be adjusted (for example by applying a Fresnel propagator) to account for the SPP diffractive propagation from the slits to the electron−SPP interaction area. When the correlated electron wave propagates in the electron microscope column following the interaction, it forms a coherent diffraction pattern that corresponds to the transfer function T. The joint measurement is able to filter out a specific set of $\overline{k}$ from those present in the source state S and to select a phase that produces an electron pure state. Shifting the detection point results in a different, shifted, diffraction pattern. When a series of detection points is summed incoherently or equivalently, there is no correlation between them and a standard incoherent electron wave can be constructed. This would invalidate the joint measurement scheme. It is, therefore, important that CL collection must be very selective in the direction and energy of the photon emitted by the grating.

As in the case of photons, a generalized optical path can be considered starting from the bucket detector, through the slits, toward the interaction region from which the rays follow as electron waves. The precise selection of the photon energy and momentum is equivalent to maintain the coherence of the virtual SPP source located in the bucket.

More General Joint Measurements. Joint measurement would equally work for any one-dimensional object with transmission function $T(y)$ (in the $x−y$ plane) instead of the two slits. For example, it would work for a phase object that imparts an effective phase shift on the electron waves.

Figure 2 shows an application to a relevant situation, where the object to be observed is a biological molecule. In this case, the SPP can excite a degree of freedom of the molecule, resulting in an amplitude effect. We calculated SPP scattering from a circular hole simulating the molecule approached by a non-dispersive plane wave coming from the bucket. The resulting field is shown in Figure 2b. The calculation method is detailed in the Methods Section. This is the explicit form of E^{REV}: when the electron beam interacts with the slab in the rectangular area, this represents the solution singled out by the bucket detector. The accumulated coincident electrons form the image shown in Figure 2c. Since phase is also constrained in the coincidence, electron propagation through focus can also be used to extrapolate the SPP function outside the interaction region, as shown in Figure 2d.
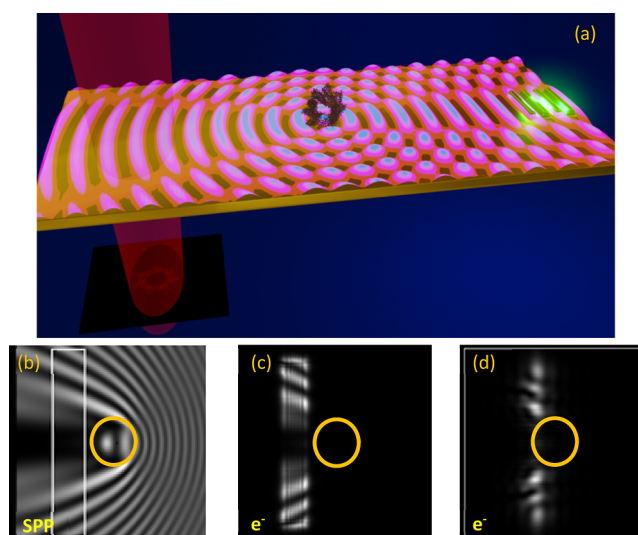

Figure 2. Ghost imaging application. (a) Schematic diagram of the application of ghost imaging to the study of electron-dose-sensitive materials such as biological molecules. The molecules interact with the electromagnetic wave, and the image is reconstructed on the electron beam by performing a joint measurement with a bucket detector on the SPP side. (b−d) Simulation of ghost imaging: (b) solution for the field of a propagating wave departing from a far source/detector on the left outside the image and encountering a cylindrical hole. The phase and amplitude have been matched in the interaction area with the electron beam, indicated here as a rectangle. (c) Coincident electron forms an image on the screen. When imaged out of focus, different parts of the SPP electromagnetic wave can be extrapolated to the molecule sides (d).

The presence of the molecule in the slab can also result in a local change in refractive index as a phase effect. The technique is similar to surface plasmon resonance (SPR), but with very high spatial resolution, simultaneously providing a well-defined phase and "imaging" sensitivity.[41] The ability to image molecules exploiting the SPP-induced interaction[42] to reduce damage induced by direct electron beam irradiation is a very relevant research theme.[43] It provides an innovative approach for imaging electron-dose-sensitive objects. The spatial resolution is dictated either by the SPP wavelength or by the distance D between the electron beam interaction area and the object. It is reasonable to infer that, if D is smaller than the decay length of the near field induced by the electron beam, the resolution can be pushed far below the SPP wavelength.

In a realistic case, limitations to the resolution may arise from the finite size of the grating, its effective coherence as a virtual source of SPPs, and its distance. As in any optical system, the highest resolution can be obtained at the cost of intensity, which is the coincidence rate in this case.

If scattering between the SPP and the molecule is only elastic, then probing is damage-free. Considering instead excitation of a molecule via the SPP interaction, the experiment is similar, in terms of dose, to vibrational electron energy-loss spectroscopy (EELS) in an "aloof" configuration (i.e., with an electron trajectory not directly on the sample), which reduces damage by orders of magnitude.[44] To be more precise as stated in ref 44 if the electron hits the metallic slab, it generates a wealth of highly energetic signals, which can potentially damage delicate samples on the slab. To avoid this, the distance D of the molecule must be carefully chosen and even an "aloof" joint measurement could be considered.

In view of these considerations, a resolution better than 10–20 nm (see Supporting Information) should be achievable and could be potentially increased with phase reconstruction techniques. In this sense, there is a potential to equal or surpass, in terms of resolution, the best nearfield resolution.

Due to the synchronous and phase locked nature of the measurement, it is natural to expect an information/dose advantage for ghost imaging with respect to both standard EELS and near field optical techniques. In view of the above "reciprocity" scheme, the proposed 1D "ghost imaging" scheme can be considered as the time reverse of a PINEM mechanism (see Figure 3). This scheme was, for instance, used
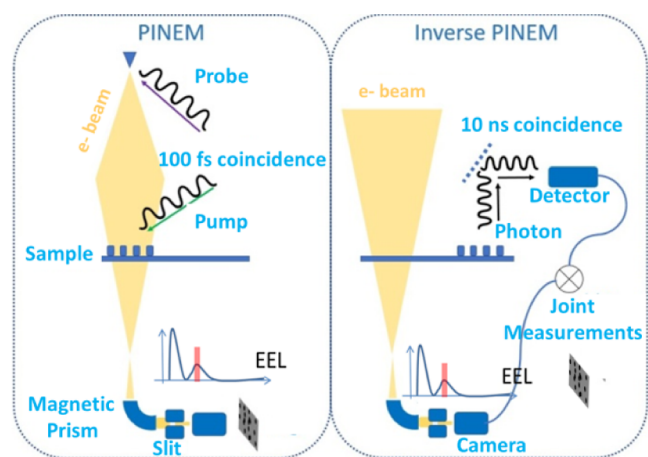

Figure 3. Experimental setup. Schematic diagrams showing a comparison between PINEM based on ultrafast TEM and inverse PINEM based on one-dimensional ghost imaging.

to generate ultrafast electron vortex beams with structured SPPs.[29] Reversing the coincidence between the electron and the cathodoluminescence light, which was previously emitted by the gratings, leads to photon excitation distinctive of the PINEM interaction (Figure 3).

Experimental Feasibility Considerations. The advancement of fast cameras, event-based detection, and coincidence has been demonstrated by several recent experiments.[36,45–48] These recent realizations strengthen the feasibility of the experiment we propose here. We notice, in particular, that the independently developed approaches in refs [36] and [48] hinge on the quantum character of the coincidence, similar to what was proposed in our work at about the same time.[49] A reverse PINEM method would present several advantages experimentally, since it does not require the use of a pulsed electron beam, but only a joint measurement. Here, the difficulty lies in the ability to collect light efficiently, to use single photon detectors, and to synchronize them with event-driven cameras, enabling joint measurements between electrons and photons and repeating the process for all other spurious events. The recording of joint measurements with a camera, i.e., being able to collect coincident events spatially and temporally, is an existing technology.[45,48] The rate of electron emission per second can be linked to the electron current by the relation, $n = i_e/e$. For a monochromated electron beam, almost all inelastic events associated with SPP creation correspond to a fraction P_{SPP} of the full electron beam falling on a selected electron energy window. P_{SPP} could be modified to account for the electron detection efficiency. On average, an electron reaches an energy-filtered TEM image every $\tau_{spp} = e/(i_e P_{SPP})$.

Given the use of post selection on a grating, "suitable" photons for coincidence are emitted with probability $P_{PS} = |c|^2|a|^2$, where a is the coefficient of k decomposition for SPP generation in eq 1 and c is the superposition integral for the direct and reverse field in eq 4. The factor a can be modified to evaluate the coupling strength to impinging electrons. An approximate evaluation of $|c|^2|a|^2$ can be obtained by considering the fraction of the full 2π angle for which the two slits are observed from the source and from the bucket detector (i.e., the grating). For example, if one assumes that the slits have a size of 1–2 μm and are located 5 μm from the injection area and 10 μm from the bucket, then $P_{PS} \approx 10^{-3}$ of the coincidence SPP revealed on the bucket.

An effective coincidence experiment should rely on a coincidence window of τ_{spp} and a dead time before a new acquisition of $\tau_{ps} = e/(i_e P_{SPP} P_{PS})$ (where τ_{ps} is the average time between two events in a joint measurement). For a current of 10 pA and $P_{SPP} = 0.1\%$, the required coincidence window is ~10 ns, while the dead time can be as slow as 10 μs. Faster response times, down to a few ps, would be advantageous for reducing the dark current in the detectors.

For example, the mentioned Timepix technology allows for time resolution in the ns regime or better.[46–48]

In general, schemes can be based on the acquisition of all energy-filtered TEM electrons with a time stamp placed on each of them, rejecting non-coincident events afterward.

In cases for which the detection is slow, the experiment can be improved by shaping the electron wave before interaction to increase the factor $|a|^2$. A variation of the experiment can be performed by placing the slits in the path of the electron beam instead of that of the SPP. The joint measurement can then be performed similarly to that described above and according to an inverse-PINEM perspective, with rays starting from the bucket detector and ending in the electron path. While it is well known that, for well-separated slits (e.g., more than 100 nm), the coherence of an inelastically scattered electron is negligible and no interference is expected, a joint measurement permits recovery of the interference figure in the appropriate subset of electrons.

Conditional Beam Shaping. We take the advantage of the fact that this technique is a reverse version of PINEM to describe its use for dynamic electron beam shaping.[29,50] Instead of changing the electron wavefunction using a light-driven excitation, the electron beam component is singled out by appropriate post-selection of the final state. Since more orthogonal selection channels are possible, it is also possible to imagine performing "conditional" beam shaping, whereby the shape of the beam is not "decided" until the photon is measured. There are many ways to post-select an electron state based on a selected photon state coincidence. In principle, any PINEM-based beam shaping recipe can be applied in reverse. For instance, one can consider structuring the electron beam by replacing the two slits with more complicated patterns.

Since the process is a reverse version of PINEM, the coupling is the same as for interaction with a single SPP

$$T_e = J_1(\beta)e^{i\arg(-\beta)} \approx \beta^* \tag{8}$$

$$\beta = \frac{e}{\hbar\omega_0}\int_{-\infty}^{+\infty} E_z(R, z)e^{i\omega_0 z/v}dz \tag{9}$$

where $J_1(\beta)$ is a first order Bessel function of the first kind and arg(.) is the argument. 9 are valid for the case of small

coupling, where a single SPP energy-loss band in the final state of the electron and photon is selected. For such a case, the electron transmission function is the complex conjugate of β (here, labeled β^*). For a "well-behaved" z dependence of the field, the equations restate the considerations of momentum conservation that led to eq 1. The detection should be structured in such a way as to filter only the appropriate E_z field with the phase.

As an example of electron beam shaping, we choose electron vortex beam generation and make use of the PINEM recipe from Vanacore et al.[29] By making use of a circular hole that acts as discontinuity in a metal slab, circular polarization of the impinging light beam is transformed into orbital angular momentum of the electron beam, i.e., into a vortex shaped β.

In our simulation, we substituted a single hole with a series of concentric metallic rings separated by λ_{SPP}. Figure 4 shows that this geometry has the same effect as a single hole, although it allows for a greater coupling and better energy selectivity.
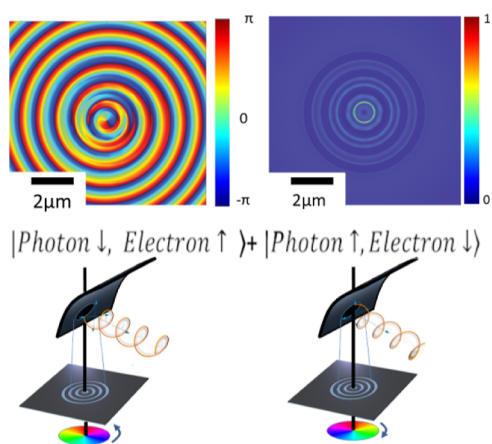

Figure 4. Example of conditional beam shaping. The structure is a metallic slab patterned with concentric rings. The upper figures show the phase (left) and amplitude (right) of the reverse solution E^{REV} (see Methods Section). The lower figures show graphical representations of the states Ψ of the systems. The electron beam is in an undetermined state between two opposite vortices. The electron state is defined only after measurement of the photon.

In the reverse situation, when the electron beam encounters a circular hole, a significant fraction of the inelastically scattered part of the electron beam goes into the SPP channel that has a vortex phase modulation (which is a solution of the Maxwell equations for this structure) and becomes correlated with the emitted light. In comparison to the first "1D ghost imaging" experiment discussed above, the grating is replaced by a circular resonator of concentric rings, where the discontinuity allows direct coupling with the unbound radiation. Within this limit, $l = +1$ is connected to the specific circular polarization, whereas $l = -1$ is associated with the other. If the slab is positioned in the illumination/condenser region of the microscope, then experiments can be performed with both vortex helicities simultaneously with a coincidence stamp added to each electron. A further development of this experiment can be considered, where the photon state is not collapsed but is re-interfered with the beam in different parts of the microscope. This approach is not discussed here.

DISCUSSION AND CONCLUSIONS

We have explored a new scheme for imaging based on a joint measurement between collective modes produced by electron–specimen interactions in an electron microscope and corresponding inelastically-scattered electrons. Such a joint measurement promises to provide a new way to reconsider coherence in inelastic scattering, permitting an increase in the amount of information extracted from each electron incident on a sample. At the same time, coincidence (e.g., between EELS and CL) on the nanosecond time scale with a ghost imaging scheme can replace many photocathode-based ultrafast TEM experiments, with advantages in electron beam coherence. The concept of ghost imaging can be used to examine electron-beam-sensitive materials without the electron beam directly impinging on them. The closest optical technique is SPR, but the fact that molecules can be spatially located and a line profile can be observed makes it superior. The resolution can also be made to be much smaller than the wavelength of the collective mode excitation. Furthermore, the approach can be used for beam shaping, with each post selection of a specific photon state corresponding to a different electron beam shape. It promises to open the way to the development of ghost imaging and interaction-free electron imaging techniques in electron microscopy, as well as the exploration of characteristic quantum phenomena and the verification of fundamental quantum effects in an electron microscope, e.g., the bell inequality.[51,52]

METHODS

The ghost imaging process presented here, which relies on a direct process whereby an electron creates SPPs that then irradiate light, is complicated to calculate. Therefore, we used the reverse approach. Calculations leading to Figure 2a are based on the analytical solution of the scattering of a plane wave through a hole, as calculated using the Mie Theory in ref 53 and implemented in MATLAB using MatScat. In page 194, the exact solution to the electromagnetic problem of absorption and scattering by an infinitely long circular cylinder is presented. The amplitude scattering matrix derived in this book is implemented in MatScat. We considered the solution for a 100 nm diameter, with a real refractive index of 2 and a λ = 800 nm, incident perpendicularly with respect to the axis of the cylinder.

This approach mimics a propagative electromagnetic solution in a planar geometry. Assuming coupling as in eqs 7 and 8, we could calculate electron propagation for different levels of electron lens defocus.

As explained in the text, this corresponds to a stationary solution that we assumed to be valid also as E^{REV} after conjugation.

Note that for the electrons, the propagation was described in parabolic approximation. Figure 4 was calculated using Ansys Lumerical FDTD, considering a circularly polarized laser excitation (λ = 800 nm) of a nanohole and concentric circular engravings (Si_3N_4 on Silver substrate). The nanohole has a diameter equal to the laser wavelength (800 nm), while other engravings have a regular spacing equal to λ_{SPP} = 708 nm, intended as the distance between the outer radius of the Si_3N_4 etchings. The structure is shown in Figure 5.

The reverse field E^{REV} was calculated based on the illumination of the membrane by circularly polarized light, which produced an SPP field carrying orbital angular
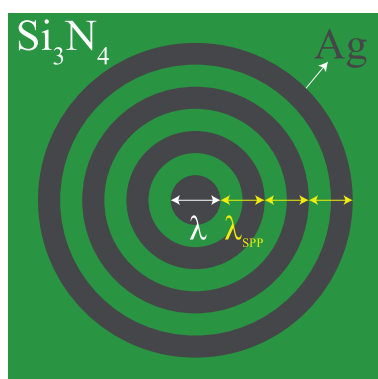
Figure 5. Scheme of the structure for the experiment in Figure 4.

momentum. The subsequent interaction with the electron beam was then based on a combination of inverse transition radiation and near-field coupling.

ASSOCIATED CONTENT

Supporting Information

The Supporting Information is available free of charge at https://pubs.acs.org/doi/10.1021/acsphotonics.2c01925.

> Resolution considerations: the relation between the resolution and probe/sample distance (PDF)

AUTHOR INFORMATION

Corresponding Author

Vincenzo Grillo − *Centro S3, Istituto di Nanoscienze-CNR, 41125 Modena, Italy;* orcid.org/0000-0002-0389-7664; Email: vincenzo.grillo@nano.cnr.it

Authors

Enzo Rotunno − *Centro S3, Istituto di Nanoscienze-CNR, 41125 Modena, Italy;* orcid.org/0000-0003-1313-3884

Simone Gargiulo − *Institute of Physics, Laboratory for Ultrafast Microscopy and Electron Scattering (LUMES), École Polytechnique Fédérale de Lausanne, Lausanne 1015, Switzerland;* orcid.org/0000-0002-7820-3372

Giovanni M. Vanacore − *Department of Materials Science, University of Milano-Bicocca, Milano 20121, Italy;* orcid.org/0000-0002-7228-7982

Chen Mechel − *Department of Electrical Engineering, Technion-Israel Institute of Technology, Haifa 32000, Israel*

Amir H. Tavabi − *Ernst Ruska-Centre for Microscopy and Spectroscopy with Electrons and Peter Grünberg Institute, Jülich 52425, Germany;* orcid.org/0000-0003-1551-885X

Rafal E. Dunin-Borkowski − *Ernst Ruska-Centre for Microscopy and Spectroscopy with Electrons and Peter Grünberg Institute, Jülich 52425, Germany;* orcid.org/0000-0001-8082-0647

Fabrizio Carbone − *Institute of Physics, Laboratory for Ultrafast Microscopy and Electron Scattering (LUMES), École Polytechnique Fédérale de Lausanne, Lausanne 1015, Switzerland*

Ivan Madan − *Institute of Physics, Laboratory for Ultrafast Microscopy and Electron Scattering (LUMES), École Polytechnique Fédérale de Lausanne, Lausanne 1015, Switzerland;* orcid.org/0000-0002-0137-8537

Stefano Frabboni − *Dipartimento FIM, Universitá di Modena e Reggio Emilia, Modena 41125, Italy*

Tugrul Guner − *Department of Physics, University of Ottawa, Ottawa, Ontario K1N 6N5, Canada;* orcid.org/0000-0001-7899-0874

Ebrahim Karimi − *Department of Physics, University of Ottawa, Ottawa, Ontario K1N 6N5, Canada*

Ido Kaminer − *Department of Electrical Engineering, Technion-Israel Institute of Technology, Haifa 32000, Israel;* orcid.org/0000-0003-2691-1892

Complete contact information is available at:
https://pubs.acs.org/10.1021/acsphotonics.2c01925

Author Contributions

[∇]E.R. and S.G. contributing equally. Conceptualization V.G.; writing original draft V.G., E.K., I.K., G.M.V., and E.R.; writing, review, and editing F.C., I.M., S.F., A.H.T., and R.E.D.-B; visualization E.R., S.G., T.G. , G.M.V., and V.G.; formal analysis S.G., V.G., I.K., M.C., G.M.V., and E.R.

Notes

The authors declare no competing financial interest.

ACKNOWLEDGMENTS

REFERENCES

(1) Zurek, W. *Decoherence and the Transition from Quantum to Classical—Revisited*. Los Alamos Science Number 2002, 27, 2.

(2) Hornberger, K.; Uttenthaler, S.; Brezger, B.; Hackermüller, L.; Arndt, M.; Zeilinger, A. Collisional decoherence observed in matter wave interferometry. *Phys. Rev. Lett.* 2003, 90, 160401.

(3) Zurek, W. H. Decoherence, einselection, and the quantum origins of the classical. *Rev. Mod. Phys.* 2003, 75, 715−775.

(4) Bouchard, F.; Harris, J.; Mand, H.; Bent, N.; Santamato, E.; Boyd, R. W.; Karimi, E. Observation of quantum recoherence of photons by spatial propagation. *Sci. Rep.* 2015, 5, 15330.

(5) Venkatraman, K.; Levin, B. D. A.; March, K.; Rez, P.; Crozier, P. A. Vibrational spectroscopy at atomic resolution with electron impact scattering. *Nat. Phys.* 2019, 15, 1237−1241.

(6) Verbeeck, J.; van Dyck, D.; Lichte, H.; Potapov, P.; Schattschneider, P. Plasmon holographic experiments: theoretical framework. *Ultramicroscopy* 2005, 102, 239−255.

(7) Schattschneider, P.; Lichte, H. Correlation and the density-matrix approach to inelastic electron holography in solid state plasmas. *Phys. Rev. B* 2005, 71, 045130.

(8) Harscher, A.; Lichte, H.; Mayer, J. Interference experiments with energy filtered electrons. *Ultramicroscopy* 1997, 69, 201−209.

(9) Lichte, H.; Freitag, B. Inelastic electron holography. *Ultramicroscopy* 2000, 81, 177−186.

(10) Potapov, P.; Lichte, H.; Verbeeck, J.; van Dyck, D. Experiments on inelastic electron holography. *Ultramicroscopy* 2006, 106, 1012−1018.

(11) Potapov, P. L.; Verbeeck, J.; Schattschneider, P.; Lichte, H.; van Dyck, D. Inelastic electron holography as a variant of the Feynman thought experiment. *Ultramicroscopy* 2007, 107, 559−567.

(12) Röder, F.; Lichte, H. Inelastic electron holography -first results with surface plasmons. *Eur. Phys. J. Appl. Phys.* 2011, 54, 33504.

(13) Mechel, C.; Kurman, Y.; Karnieli, A.; Rivera, N.; Arie, A.; Kaminer, I. Quantum correlations in electron microscopy. *Optica* **2021**, *8*, 70.

(14) Egerton, R. F. Electron energy-loss spectroscopy in the TEM. *Rep. Prog. Phys.* **2008**, *72*, 016502.

(15) Schattschneider, P.; Löffler, S. Entanglement and decoherence in electron microscopy. *Ultramicroscopy* **2018**, *190*, 39−44.

(16) Pittman, T. B.; Shih, Y. H.; Strekalov, D. V.; Sergienko, A. V. Optical imaging by means of two-photon quantum entanglement. *Phys. Rev. A* **1995**, *52*, 3429−3432.

(17) Einstein, A.; Podolsky, B.; Rosen, N. Can Quantum-Mechanical Description of Physical Reality Be Considered Complete? *Phys. Rev.* **1935**, *47*, 777−780.

(18) Zeilinger, A. Experiment and the foundations of quantum physics. *Rev. Mod. Phys.* **1999**, *71*, S288−S297.

(19) Paneru, D.; Cohen, E.; Fickler, R.; Boyd, R. W.; Karimi, E. quantum or classical. *Rep. Prog. Phys.* **2020**, *83*, 064001.

(20) Popper, K. R.; v Weizsäcker. Zur Kritik der Ungenauigkeitsrelationen. *Naturwissenshaften* **1934**, *22*, 807−808.

(21) Bennink, R. S.; Bentley, S. J.; Boyd, R. W. 'Two-photon' coincidence imaging with a classical source. *Phys. Rev. Lett.* **2002**, *89*, 113601.

(22) Leifer, M. S.; Pusey, M. F. Is a time symmetric interpretation of quantum theory possible without retrocausality? *Proc. R. Soc. A* **2017**, *473*, 20160607.

(23) Cramer, J. G. The transactional interpretation of quantum mechanics. *Rev. Mod. Phys.* **1986**, *58*, 647−687.

(24) Padgett, M. J.; Boyd, R. W. An introduction to ghost imaging: quantum and classical. *Philos. Trans. R. Soc., A* **2017**, *375*, 20160233.

(25) Gatti, A.; Brambilla, E.; Bache, M.; Lugiato, L. A. Ghost imaging with thermal light: comparing entanglement and classical correlation. *Phys. Rev. Lett.* **2004**, *93*, 093602.

(26) Vanacore, G. M.; Fitzpatrick, A. W. P.; Zewail, A. H. Four-dimensional electron microscopy: Ultrafast imaging, diffraction and spectroscopy in materials science and biology. *Nano Today* **2016**, *11*, 228−249.

(27) Barwick, B.; Zewail, A. H. Photonics and plasmonics in 4D ultrafast electron microscopy. *ACS Photonics* **2015**, *2*, 1391−1402.

(28) Park, S. T.; Lin, M.; Zewail, A. H. Photon-induced near-field electron microscopy (PINEM): theoretical and experimental. *New J. Phys.* **2010**, *12*, 123028.

(29) Vanacore, G. M.; Berruto, G.; Madan, I.; Pomarico, E.; Biagioni, P.; Lamb, R. J.; McGrouther, D.; Reinhardt, O.; Kaminer, I.; Barwick, B.; Larocque, H.; Grillo, V.; Karimi, E.; García de Abajo, F. J.; Carbone, F. Ultrafast generation and control of an electron vortex beam via chiral plasmonic near fields. *Nat. Mater.* **2019**, *18*, 573−579.

(30) Zia, R.; Brongersma, M. Surface plasmon polariton analogue to Young's double-slit experiment. *Nat. Nanotechnol.* **2007**, *2*, 426−429.

(31) Bashevoy, M. V.; Jonsson, F.; MacDonald, K. F.; Chen, Y.; Zheludev, N. I. Hyperspectral imaging of plasmonic nanostructures with nanoscale resolution. *Opt. Express* **2007**, *15*, 11313.

(32) Kfir, O.; Di Giulio, V.; García de Abajo, F. J.; Ropers, C. Optical coherence transfer mediated by free electrons. *Sci. Adv.* **2021**, *7*, No. eabf6380.

(33) Feist, A.; Echternkamp, K.; Schauss, J.; Yalunin, S. V.; Schäfer, S.; Ropers, C. Quantum coherent optical phase modulation in an ultrafast transmission electron microscope. *Nature* **2015**, *521*, 200−203.

(34) Vanacore, G. M.; Madan, I.; Berruto, G.; Wang, K.; Pomarico, E.; Lamb, R. J.; McGrouther, D.; Kaminer, I.; Barwick, B.; García de Abajo, F. J.; Carbone, F. Attosecond coherent control of free-electron wave functions using semi-infinite light fields. *Nat. Comput.* **2018**, *9*, 2694.

(35) Karnieli, A.; Rivera, N.; Arie, A.; Kaminer, I. The coherence of light is fundamentally tied to the quantum coherence of the emitting particle. *Sci. Adv.* **2021**, *7*, No. eabf8096.

(36) Feist, A.; Huang, G.; Arend, G.; Yang, Y.; Henke, J. W.; Raja, A. S.; Kappert, F. J.; Wang, R. N.; Lourenço-Martins, H.; Qiu, Z.; Liu, J.; Kfir, O.; Kippenberg, T. J.; Ropers, C. Cavity-mediated electron-photon pairs. *Science* **2022**, *377*, 777−780.

(37) Rivera, N.; Kaminer, I. Light-matter interactions with photonic quasiparticles. *Nat. Rev. Phys.* **2020**, *2*, 538−561.

(38) García de Abajo, F. J.; Asenjo-Garcia, A.; Kociak, M. Multiphoton Absorption and Emission by Interaction of Swift Electrons with Evanescent Light Fields. *Nano Lett.* **2010**, *10*, 1859−1863.

(39) Pomarico, E.; Madan, I.; Berruto, G.; Vanacore, G. M.; Wang, K.; Kaminer, I.; García de Abajo, F. J.; Carbone, F. meV Resolution in Laser-Assisted Energy-Filtered Transmission Electron Microscopy. *ACS Photonics* **2018**, *5*, 759−764.

(40) García de Abajo, F. J. Optical excitations in electron microscopy. *Rev. Mod. Phys.* **2010**, *82*, 209−275.

(41) Tokel, O.; Yildiz, U. H.; Inci, F.; Durmus, N. G.; Ekiz, O. O.; Turker, B.; Cetin, C.; Rao, S.; Sridhar, K.; Natarajan, N.; et al. Portable microfluidic integrated plasmonic platform for pathogen detection. *Sci. Rep.* **2015**, *5*, 9152.

(42) Marchand, R.; Sachl, R.; Kalbac, M.; Hof, M.; Tromp, R.; Amaro, M.; van der Molen, S. J.; Juffmann, T. Optical Near-Field Electron Microscopy. *Phys. Rev. Appl.* **2021**, *16*, 014008.

(43) Henderson, R. The potential and limitations of neutrons, electrons and X-rays for atomic resolution microscopy of unstained biological molecules. *Q. Rev. Biophys.* **1995**, *28*, 171−193.

(44) Rez, P.; Aoki, T.; March, K.; Gur, D.; Krivanek, O. L.; Dellby, N.; Lovejoy, T. C.; Wolf, S. G.; Cohen, H. Damage-free vibrational spectroscopy of biological materials in the electron microscope. *Nat. Commun.* **2016**, *7*, 10945.

(45) Jannis, D.; Müller-Caspary, K.; Béché, A.; Oelsner, A.; Verbeeck, J. Spectroscopic coincidence experiments in transmission electron microscopy. *Appl. Phys. Lett.* **2019**, *114*, 143101.

(46) Jannis, D.; Hofer, C.; Gao, C.; Xie, X.; Béché, A.; Pennycook, T. J.; Verbeeck, J. Event driven 4D STEM acquisition with a Timepix3 detector: Microsecond dwell time and faster scans for high precision and low dose applications. *Ultramicroscopy* **2022**, *233*, 113423.

(47) Auad, Y.; Walls, M.; Blazit, J.-D.; Stéphan, O.; Tizei, L. H. G.; Kociak, M.; De la Peña, F.; Tencé, M. Event-based hyperspectral EELS: towards nanosecond temporal resolution. *Ultramicroscopy* **2022**, *239*, 113539.

(48) Varkentina, N.; Auad, Y.; Woo, S. Y.; Zobelli, A.; Bocher, L.; Blazit, J.-D.; Li, X.; Tencé, M.; Watanabe, K. T. T.; Stéphan, O.; Kociak, M.; Tizei, L. H. G. Cathodoluminescence excitation spectroscopy: Nanoscale imaging of excitation pathways. *Sci. Adv.* **2022**, *8*, No. eabq4947.

(49) Rotunno, E.; Gargiulo, S.; Vanacore, G. M.; Mechel, C.; Tavabi, A.; E Dunin Borkowski, R.; Carbone, F.; Madan, I.; Zanfrognini, M.; Frabboni, S.; Guner, T.; Karimi, E.; Kaminer, I.; Grillo, V. One-dimensional ghost imaging with an electron microscope: a route towards ghost imaging with inelastically scattered electrons, 2021. arXiv:2106.08955. https://doi.org/10.48550/arXiv.2106.08955 (accessed Aug 8, 2021).

(50) Konecna, A.; de Abajo, F. J. G. Electron Beam Aberration Correction Using Optical Near Fields. *Phys. Rev. Lett.* **2020**, *125*, 030801.

(51) Greenberger, D. M.; Horne, M. A.; Zeilinger, A. Multiparticle interferometry and the superposition principle. *Phys. Today* **1993**, *46*, 22−29.

(52) Aspect, A.; Grangier, P.; Roger, G. Experimental Tests of Realistic Local Theories via Bell's Theorem. *Phys. Rev. Lett.* **1981**, *47*, 460−463.

(53) Bohren, C. F.; Huffman, D. R. *Absorption and Scattering of Light by Small Particles*; Wiley: New York, 1983.